Koc. J. Sci. Eng., 7(2): (2024) 184-190 https://doi.org/10.34088/kojose.1387787

Kocaeli University

Kocaeli Journal of Science and Engineering

http://dergipark.org.tr/kojose

Nanomechanical Behavior of Top and Bond Layer in TBC

Müge AKDEMİR [1,*], Merve CANBOLAT [2], Serra BAYRAM [3], Yasemin KILIÇ [4], Ahmet Arda İNCEYER [5], Hüseyin AYDIN [6], Hüseyin ÇİMENOĞLU [7]

[1] *Department of Metallurgical and Materials Engineering, İstanbul Technical University, İstanbul, 34467, Turkey,* ***ORCID:*** *0000-0001-8340-5705*
[2] *Department of Materials, Science and Engineering, Gebze Technical University, Kocaeli, 41400, Turkey,* ***ORCID:*** *0000-0001-5043-2184*
[3] *Department of Metallurgical and Materials Engineering, İstanbul Technical University, İstanbul, 34467, Turkey,* ***ORCID:*** *0009-0006-4580-5015*
[4] *Metallic Materials Technologies Research Group, TUBITAK MAM, 41470, Turkey,* ***ORCID:*** *0000-0002-9742-1826*
[5] *Metallic Materials Technologies Research Group, TUBITAK MAM, 41470, Turkey,* ***ORCID:*** *0000-0001-8086-1406*
[6] *Metallic Materials Technologies Research Group, TUBITAK MAM, 41470, Turkey,* ***ORCID:*** *0000-0002-8600-2984*
[7] *Department of Metallurgical and Materials Engineering, İstanbul Technical University, İstanbul, 34467, Turkey,* ***ORCID:*** *0000-0002-9921-7108*

Article Info

Research paper

Received : *November 15, 2023*
Accepted : *July 8, 2024*

Keywords

Thermal barrier coating,
Aluminide coating,
EB-PVD YSZ coating,
Nanoindentation,
Microstructure

Abstract

Thermal barrier coatings (TBC) have been developed to reduce the surface temperature of hot components in gas turbine engines. To get superior oxidation and mechanical properties, "The Yttria Stabilized Zirconia (YSZ)" top coat and β-NiAl bond coat are deposited by Electron Beam Physical Vapor Deposition (EB-PVD) and Chemical Vapor Deposition (CVD) processes, respectively. In this study, after structural characterization of the TBC formed on the directionally solidified (DS) CM247LC superalloy, the nanomechanical properties of the top and bond coats were determined using the nanoindentation technique. The results showed no significant differences in their elastic modulus despite the more than two times higher hardness of the top coat than the bond coat (18.4 GPa and 7.2 GPa, respectively). Energy Dispersive Spectrometry (EDS) equipped with Scanning Electron Microscope examinations revealed that Al and N- and N-rich zones within the bond coat have an underlying diffusion zone. In addition, thermal-grown oxide (TGO) film was detected at the interface of the top and bond coat.

1. Introduction

Gas turbine engines operate under extreme conditions such as elevated temperatures, high pressure, and corrosive environments. Directional solidified and single-crystal nickel-based superalloys are designed to meet the creep and fatigue requirements of turbine engines. Although single crystals (SX) superalloys have higher creep and hot corrosion resistance compared to directional solidified (DS) superalloys, DS alloys are the material of choice for rotating parts, blades, and wheels such as 2nd and 3rd stage turbine parts due to cost-effective compositions and casting processes. In addition to their superior strength, they require protection from a hot corrosive environment. Thermal barrier coatings (TBCs) are applied to reduce excessive heat flow, reaching up to 1650°C during operation, and they aim to protect the superalloy parts from oxidation and corrosion.

1.1. TBCs for Gas Turbine Engines

TBCs consist of two main regions: the top coat for reducing the metal temperature and the bond coat for oxidation protection of the underlying superalloy. Besides the oxidation protection, the bond coat plays an important role in eliminating the coating failures arising from the thermal expansion coefficient difference between the top coat and substrate. In industrial applications, the bond coat could made up of MCrAlYX (M = Ni, Co; X = Si, Hf) or aluminide (β-NiAl, (Ni, Pt) Al, etc.). Among the bond coatings, (NiAl) type aluminides exhibit superior adhesion, higher melting point, lower density, and better oxidation resistance.

In the TBC system, the bond coat is deposited with the CVD process, which provides opportunities like controlling process parameters, growth rate, and microstructure of coating, as well as obtaining uniform

* Corresponding Author: akdemirmug@itu.edu.tr
This article was presented as an oral presentation at the 3rd International Characterization Symposium held in Istanbul between 6-8 September 2023.

coating thickness in complex geometries such as turbine blades. As the top coat of TBCs, mostly partially yttrium-stabilized zirconia (YSZ) containing 6-8%wt yttria is deposited over the bond coating by atmospheric plasma spray (APS) or electron beam physical vapor deposition (EB-PVD) methods. The YSZ coat deposited via EB-PVD has several advantages over APS, including good surface properties, higher strain tolerance, and oxygen permeability due to its porous and columnar structure [1–7].

The properties of TBC systems are critical for the lifetime of turbine blades. Delamination of coating layers due to thermal expansion, hot corrosion, and erosion for the ceramic top coat are the primary failure modes. For the metallic bond coat, degradation of the structure, thermal fatigue cracking, oxidation, and hot corrosion determine the lifetime [2]. The mechanical properties of TBC should be higher but compatible with the substrate alloy. Measuring the mechanical properties of coatings apart from the influence of substrate alloy is possible with the nanoindentation technique. The relatively low thicknesses of the top coat (~100μm) and bond coat (~60 μm) and their complex microstructure handicap the accurate measurement by standard mechanical testing.

1.2. Nanoindentation Studies on TBCs

Numerous studies have investigated the mechanical durability of different coats of TBC materials by using nanoindentation techniques such as fracture toughness, thermal cycling behavior, impact resistance, and erosion behavior [8–11]. The effect of the chemical composition of YSZ EB-PVD coating on the wear resistance was investigated by Dharini et al. [12] by using the scratch mode of the nanoindentation tester. Increasing Ni content in Ni-YSZ nanocomposite coating up to 50% increased wear resistance and reduced internal stress and thermal expansion. Not only the chemical composition but also the post-heat treatment has substantial effects on TBC properties. Jang et al. [13] reported that soaking of EB-PVD deposited YSZ top-coated components to short-term isothermal heat treatment increases the hardness and Young Modulus of the top coat, unlike the long-term heat treatment, reducing the mechanical properties. The main focus of the studies on TBCs is to investigate the effects of heat treatment and thermal cycling on their high-temperature performance. In this regard, Chen et al. [8], who examined the correlation between the nano-impact tests and the erosion behavior of EB-PVD deposited YSZ, found that the hardness and stiffness of YSZ increase, but erosion and impact resistance decrease with thermal aging.

The microstructural variations and their mechanical properties determine the lifetime of TBC, especially in the service conditions. Failures associated with service conditions are closely related to the elastic modulus and hardness of each coating layer. Discovering the link between microstructure and mechanical behavior of TBCs on DS superalloy is crucial for developing advanced materials that can withstand harsh environments. This study delves into this crucial area, offering valuable insights that can pave the way for more robust and reliable TBCs.

2. Materials and Methods

The TBC was deposited on a DS Ni-based CM247LC superalloy cast in TUBİTAK-MRC. The composition of the superalloy, having hardness (H) of 10.5 GPa and reduced elastic modulus (Er) of 232 GPa as determined by using the Berkovich indenter attached nanoindentation tester, is given in **Table 1**. As the bond coat, NiAl was deposited on DS samples via high activation and high-temperature chemical vapor deposition (CVD or Chemical Vapor Aluminizing). The CVD process consists of a coating process at 1070 °C for 6h with an Al-Cr donor material and a heat treatment process for 2h in the argon atmosphere. After the CVD coating, YSZ was coated as a top coat on the coupon samples using the EB-PVD process. The EB-PVD process was performed at 1050°C-1100°C using 7.5 %wt YSZ ingots.

TBC deposited samples were cut and mounted in bakelite for cross-section examinations after polishing with a 6 μm diamond containing solution and 0.3 μm colloidal silica by using a vibratory polisher (GIGA-0900) following the gentle grinding. Structural features of the top and bond coats were examined by using an electron dispersive spectrometry (EDS, Oxford AZtec Ultim Max 100) attached scanning electron microscope (SEM, Hitachi SU7000) and X-ray diffraction (XRD, Rigaku) analysis under Cu Kαradiation with scanning rate 1°C/min and 2θ angle between 20-100°.

Table 1. Composition of the DS alloy used in this study (wt%).

Ni	W	Co	Cr	Al
Bal.	≤9.5	≤9.5	<8.5	<6.0
Ta	Hf	Ti	Mo	Re
<3.5	<1.5	<1	<1	<0.2
C	Fe	B	Nb	Zr
<0.1	<0.05	<0.05	<0.1	<0.005

Nanoindentation tests were conducted on the cross-section of the TBC by using the Berkovich diamond indenter attached Bruker-Hysitron TI 980 Triboindenter, under load-controlled mode. The parameters of the

indentation tests conducted on the top and bond coats and the substrate are given in **Table 2**.

Table 2. Nanoindentation test parameters used in determination nanomechanical properties of the TBC.

Indentation Regions	Max. Load	Loading/Unloading Rate
Substrate (DS CM247LC)	500 μN for 5s	50 μN/s
β-NiAl Bond Coat	500 μN for 5s	50 μN/s
YSZ Top Coat	6000 μN for 5s	50 μN/s
β-NiAl Bond Coat	6000 μN for 5s	50 μN/s

3. Results and Discussion

3.1. Results of Microstructural Examination

The XRD patterns of the top and bond coats of the TBC system are shown in **Figure 1** and **Figure 2**. The XRD examinations confirmed that the top and bond coats consisted of tetragonal-structured yttrium-stabilized zirconia (t′-YSZ) and β-NiAl phases, respectively. It should be noted that t′-YSZ has higher mechanical strength than other YSZ-allotropes [14].

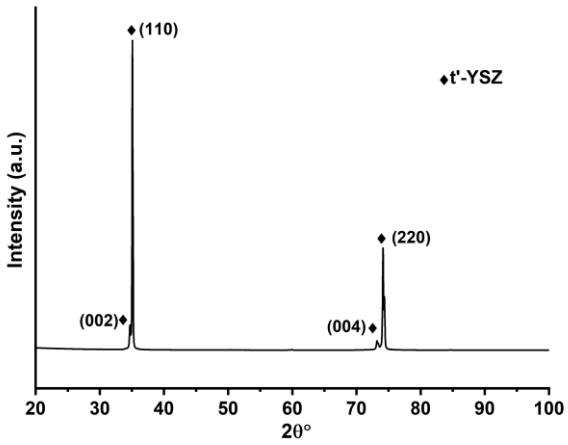

Figure 1. XRD pattern of the top coat (t′-YSZ).

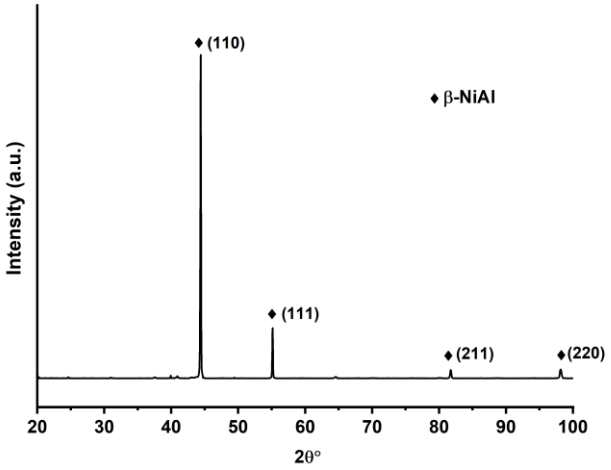

Figure 2. XRD pattern of the bond coats (β-NiAl).

Cross-section SEM images of the TBC are shown in **Figure 3**. The top coat having t′-YSZ phase structure appeared in columnar morphology over the bond coat having β-NiAl phase structure. The thicknesses of the top and bond coats were ~114 μm and ~47 μm, respectively. Considering the intensities of Al and Ni, the bond coat consisted of Al-rich and Ni-rich zones with thicknesses of ~25 μm and ~22 μm, respectively. It is a well-known fact that the thickness of the TBC coatings plays a crucial role in efficiency against thermal effects. Thus, for obtaining better thermal insulation, thicker top coats are preferred. However, thickness leads to residual stress and additional strain energy that could accelerate the coating failure [2].

For this reason, the optimum top coat thickness should be between 100-300 μm [15-18]. On the other hand, the development of a diffusion zone under the bond coat is the result of the diffusion of carbide-forming elements from the substrate towards the bond coat during the CVD process. More commonly, the structure of the diffusion zone consists of a matrix of bond coat and carbide/intermetallic precipitates [19].

Figure 4 presents the EDS elemental mapping of the TBC. It also confirmed that the columnar top coat (t′-YSZ) was rich in Zr and Y, while the bond coat (β-NiAl) was rich in Ni and Al. It is worth expressing that at the interface of top and bond coatings, Al and O-rich thin film (~2 μm) appeared as evidence of the development of TGO film. EDS elemental mapping conducted on the diffusion zone (**Figure 4**) confirmed diffusion of carbide-forming elements, including W, Ta, Hf, Cr, and C, from the substrate to the β-NiAl matrix.

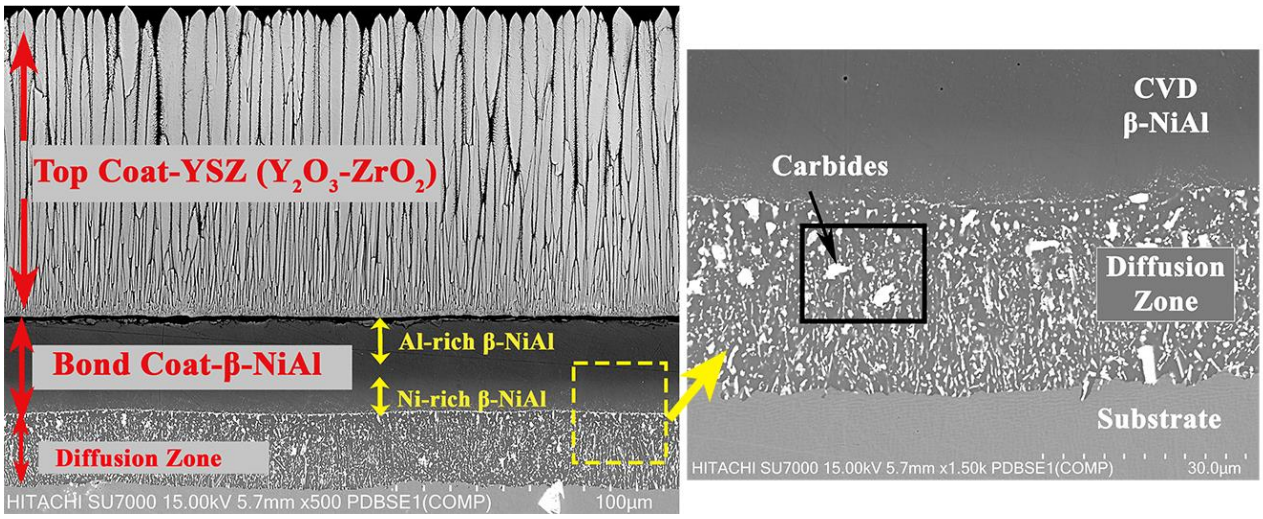

Figure 3. Cross section SEM image of the TBC fabricated on DS Ni-based CM247LC superalloy.

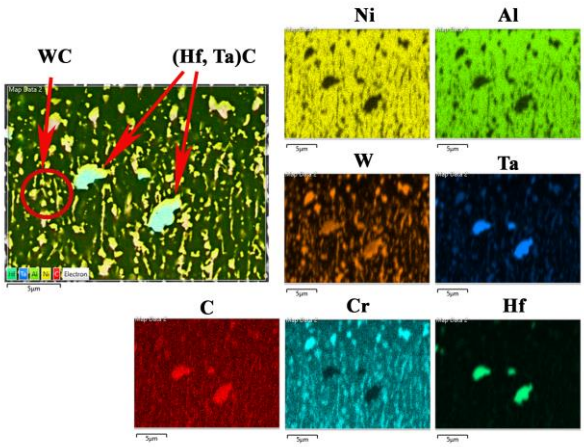

Figure 4. EDS elemental mapping alloyıng elements ın the diffusion zone.

3.2. Nanoindentation Results

Several data were collected by performing a matrix of multiple indentations from the top and the bond coats under max. indentation load (P_{max}) of 6000μN. The relevant loading-unloading curves are shown in **Figure 5**. From these curves, indentation hardness (H) and elastic modulus (E_r) were extracted according to the Oliver-Pharr [20] method (in Eq. (1) and (2));

$$H = \frac{P_{max}}{A_c} \quad (1)$$

$$E_r = \frac{\sqrt{\pi}S}{2\beta\sqrt{A_c}} \quad (2)$$

where Ac is the contact area determined from $A_c = 24.5 \times h_c^2$ considering the depth of penetration (hc) of indenter. β is the correction factor for the Berkovich tip (1.034) and S is the slope of the unloading curve.

The calculated average H and E_r values of the top and bond coats are listed in **Table 3**. In general, the top coat has more than two times higher hardness than the bond coat but their E_r values remained in a similar range. The remarkably higher hardness of the top coat than that of the bond coat can be attributed to the ceramic nature of the top coat (t′-YSZ). But its Er value in the range of the bond coat (β-NiAl) suggested that indents coincided with the porosites, which more likely develop as cooling channels in the columnar structure of YSZ [22].

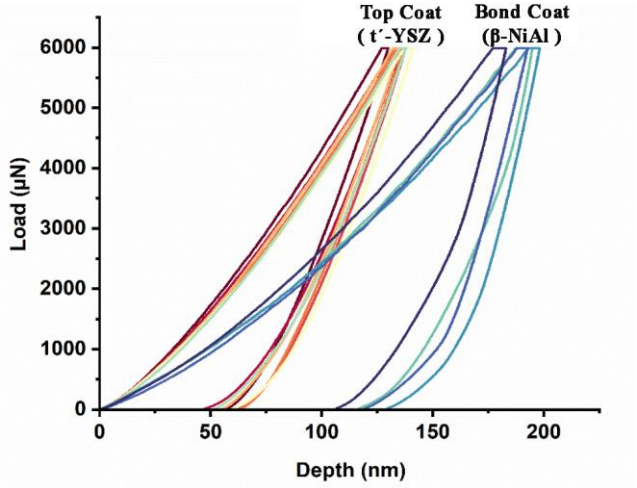

Figure 5. Loading-Unloading curves of top and bond coats.

Table 3. H and E_r values of the top and bond coats calculated from the nanoindentaion tests conducted under load of 6000 μN.

	H(GPa)	Er(GPa)
Top Coat	18.38 ± 1	167.53 ± 16.35
Bond Coat	7.23 ± 0.38	170.97 ± 21.35

Since the bond coat has Al- and Ni-rich zones (**Figure 3**), an attempt has been made to determine their

mechanical properties. For this purpose, nanoindentation tests were conducted under load of 500 µN. Representative loading-unloading indentation curves are displayed in **Figure 6**. The average H and E_r values are listed in **Table 4**. As a general trend, Al-rich zones yielded higher H and E_r than the Ni-rich zones. According to the scanning probe microscope (SPM) images given in **Figure 7**, higher H and E_r values of the Al-rich zone could be due to the presence of fine precipitates in this zone. In the previous works, the reason for the higher elastic modulus of the Al-rich zone is attributed to the increase in the binding energy of Ni-Al covalent bonds, while it decreases with lower Al concentration in the Ni-rich zone of NiAl coating according to Grimme et al. [23], Oskay et al. [24], Rusovic and Warlimont [25], Webler et al. [26], and Noebe et al. [27].

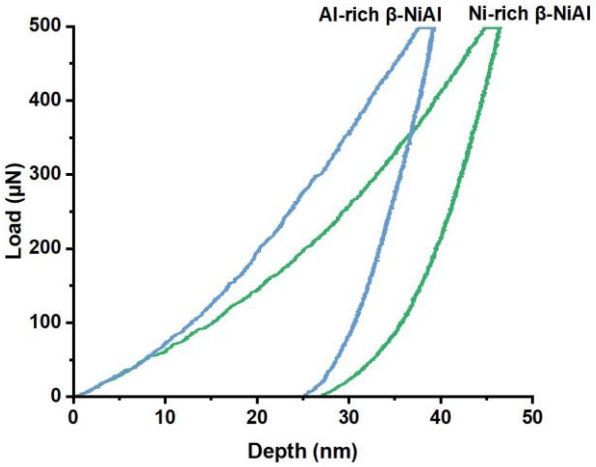

Figure 6. Loading-unloading curves of the bond coat after nanoindentation tests conducted under load of 500 µN.

Table 4. Average H and E_r values of the bond coat after indendentation tests conducted under 500 µN.

	H(GPa)	E_r(GPa)
Al-rich β-NiAl	10.21 ± 2.22	247.96 ± 20.02
Ni-rich β-NiAl	9.72 ± 0.58	197.38 ± 13.28

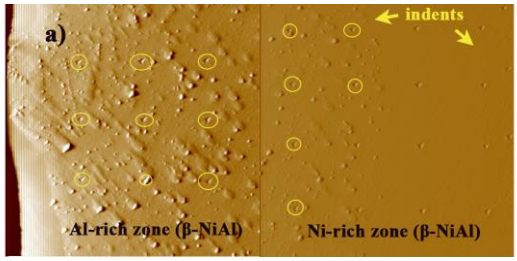

Figure 7. SPM images of the bond layer after indentation test.

In **Figure 8**, indentation loading-unloading curves obtained after conducting nanoindentation tests on the matrix and the precipitates of the diffusion zone under the load of 500 µN are presented. The calculated H and E_r values for the matrix and the precipitates are given in **Table 5**. Since the precipitates were mostly MC-type carbide (**Figure 4**), they yielded higher hardness and reduced elastic modulus than the matrix (β-NiAl).

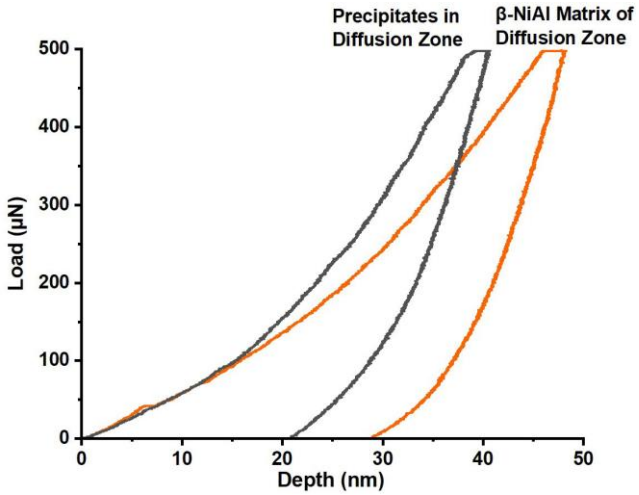

Figure 8. Loading-unloading indentation curves of the diffusion zone.

Table 5. Average H and E_r values of the diffusion zone after indendentation tests under 500 µN.

	H(GPa)	E_r(GPa)
Precipitates in Diffusion Zone	20.63 ± 4.04	261.17 ± 10.52
β-NiAl Matrix of Diffusion Zone	9.38 ± 0.48	193.02 ± 8.35

4. Conclusion

Microstructural characterizations showed that examined TBC mainly consisted of a top coat having a well-developed YSZ columnar structure and a β-NiAl bond coat containing Al- and Ni-rich zones. In between the top and bond coat, TGO film was developed. Additionally, a diffusion zone was formed under the bond coat. The structure of the diffusion zone consisted of β-NiAl Matrix and precipitates of MC-type carbides. Results of the nanoindentation tests conducted on the top coat, bond coat, and diffusion zone can be summarized as follows:

- YSZ top coat is harder than the β-NiAl bond coat but has reduced elastic modulus in the range of the β-NiAl bond coat.
- The hardness and elastic modulus of the Ni-rich zone of the bond coat (having β-NiAl structure) and the β-NiAl matrix of the diffusion zone are very close.

However, the Al-rich zone of the bond coat exhibited higher hardness and elastic modulus. Despite their lower hardness compared to the hardness of the the MC-type precipitates present in the diffusion zone, the elastic modulus of the Al-rich zone is compatible with the elastic modulus of the MC-type precipitates.

Declaration of Ethical Standards

The authors of this article declare that the materials and methods used in their studies do not require ethical committee approval and/or legal-specific permission.

Conflict of Interest

The authors declare that they have no known competing financial interests or personal relationships that could have appeared to influence the work reported in this paper.

Acknowledgements

The authors acknowledge The Scientific and Technological Research Council of Turkey, Marmara Research Center (TUBITAK MRC) for providing materials and the necessary facilities to conduct this research. The authors would also acknowledge Aylin Şahin KAHRAMAN for support in Electron Microscopy investigations.

References

[1] Wahl J.B., Harris K., 2011. Advanced Ni base superalloys for small gas turbines. Canadiand Metallurgical Quaterly, pp 207-214.

[2] Bose S., 2018. High Temperature Coatings, 2 nd ed. Elsevier.

[3] Dong H., 2010. Surface Engineering Of Light Alloys : Aluminum, Magnesium And Titanium Alloys, 1 st ed. Woodhead Pub.

[4] Chandio A.D., Abro S.H., 2018. Effect Of Temperature And Time On Nickel Aluminide Coating Deposition, Mehran University Research Journal Of Engineering And Technology, **37**, pp. 491–496.

[5] Ertürk U., 2017. Production And Development Of Aluminide Coatings By Chemical Vapor Deposition On Nickel Based Superalloys For Turbine Engine Applications. MSc Thesis, Natural And Applied Sciences Of Middle East Technical University.

[6] Zubacheva O.A., 2004. Plasma-Sprayed And Physically Vapor Deposited Thermal Barrier Coatings: Comparative Analysis Of Thermoelastic Behavior Based On Curvature Studies. PhD Thesis, RWTH Aachen University.

[7] Peters M., Leyens C., Schulz U., Kaysser W.A., 2001. Eb-Pvd Thermal Barrier Coatings For Aeroengines And Gas Turbines. Advanced Engineering Materials, **3**(4), pp. 192-204.

[8] Chen J., Beake B.D., Wellman R.G., Nicholls J.R., Dong H., 2012. An İnvestigation İnto The Correlation Between Nano-İmpact Resistance And Erosion Performance Of EB-PVD Thermal Barrier Coatings On Thermal Ageing, Surface Coating Technology. **206**(23), pp. 4992–4998.

[9] Wang X., Wang C., Atkinson A., 2012. Interface Fracture Toughness İn Thermal Barrier Coatings By Cross-Sectional İndentation, Acta Materials, **60**, pp. 6152–6163.

[10] Gabel S., Giese S., Webler R.U., Neumeier S., Göken M., 2022. Microcantilever Fracture Tests Of A-Cr Containing Nial Bond Coats, Advanced Engineering Materials, **24**(7).

[11] Xu Z., Wang Z., Huang G., Mu R., He L., 2015. Thermal Cycling Behavior Of Eb-Pvd Tbcs On Cvd Platinum Modified Aluminide Coatings, Journal of Alloys and Compounds, **637**, pp. 226–233.

[12] Dharini T., Kuppusami P., Kumar N., Kumar D.D., Soman A.K., Kirubaharan A.M.K., 2021. Tribological Properties Of Ysz And Ysz/Ni-Ysz Nanocomposite Coatings Prepared By Electron Beam Physical Vapour Deposition, Ceramics International, **47**(18), pp. 26010–26018.

[13] Jang B.K., Kim S.H., Fisher C.A.J., Kim H.T., 2022. Effect Of Isothermal Heat Treatment On Nanoindentation Hardness And Young's Modulus Of 4 Mol% Y2O3-ZrO2 EB-PVD TBCs, Materials Today Communication, 31.

[14] Song, X., Zhang, Y.D., Jiang, C., Liu, Z., Lin, C., Zheng, W. Zeng, Y., 2023. Thermophysical and mechanical properties of cubic, tetragonal and monoclinic ZrO_2. Journal of Materials Research and Technology, 23, pp. 648-655.

[15] Mahade S., 2016. Functional Performance Of Gadolinium Zirconate/Yttria Stabilized Zirconia Multi-Layered Thermal Barrier Coatings. Phd Thesis, University West, Sweden. Isbn: 978-91-87531-37-8.

[17] Vignesh B., Oliver W.C., Kumar G.S., And Phani P.S., 2019. Critical Assessment Of High Speed Nanoindentation Mapping Technique And Data Deconvolution On Thermal Barrier Coatings.

Materals and Design, **181**.

[18] Lee K.I, 1998. Protective Coatings For Gas Turbines. The Gas Turbine Handbook, Chap.4.4.2, Edited By Netl, 419-438, 2006.

[19] Pillai, R., Chyrkin, A., Grüner, D., Nowak, W., Zheng, N., Kliewe, A., Quadakkers, W.J., 2016. Carbides in an aluminised single crystal superalloy: Tracing the source of carbon. Surface and Coatings Technology, **288**, pp. 15-24.

[20] Oliver, W. C., & Pharr, G. M., 1992. An improved technique for determining hardness and elastic modulus using load and displacement sensing indentation experiments. J. Mater. Res., **7**(6), pp.1564-1583.

[21] Verma V., Patel S.,Swarnkar V., Rajput S.K., 2018. Effect Of Coating Thickness On Microstructure And Low Temperature Cyclic Thermal Fatigue Behavior Of Thermal Barrier Coating (Al_2O_3). Iop Conf. Series: Materials Science And Engineering, **330**, 012050.

[22] Pfeiffer C., Affeldt E., Göken M., 2011. Miniaturized bend tests on partially stabilized EB-PVD ZrO. thermal barrier coating. Surface and Coating Technology, **205**(10), pp. 3245-3250.

[23] Grimme C., Oskay C., Mengis L., Galetz M.C., 2021. High temperature wear behavior of δ-Ni2Al3 and β-NiAl coatings formed on pure nickel using pack cementation process and diffusion heat treatment. Wear, **477**.

[24] Oskay C., Rudolphia M., Affeldtb E.E., Schützea M., Galetz M.C., 2017. Evolution of microstructure and mechanical properties of NiAl-Diffusion coatings after thermocyclic exposure. Intermetallics, **89**, pp. 22-31.

[25] Rusovic N., Warlimont H., 1979. Young's Modulus of β2-NiAl Alloys. Physica Status Solidi (a), **53**, pp. 283.

[26] Webler R., Krottenthaler M., Neumeier S., Durst K., Goken M., 2012. Local fracture toughness and residual stress measurements on NiAl bond coats by micro cantilever and FIB-based bar milling tests, in: E.S. Huron, R.C. Reed, M.C. Hardy, M.J. Mills, R.E. Montero, P.D. Portella, J. Telesman (Eds.), Proceedings of the 12th International Symposium on Superalloys, John Wiley & Sons, Hoboken, NJ, USA, pp. 93–102.

[27] Noebe R.D., Bowman R.R., Nathal M.V., 2013. Physical and mechanical properties of the B2 compound NiAl. International Materials Review, **38**, pp. 193-232.